Available online at www.sciencedirect.com

ScienceDirect

Materials Today: Proceedings 6 (2019) 106–115

materialstoday: PROCEEDINGS

www.materialstoday.com/proceedings

3rd ISE SSRSEU 2018

β-Ni(OH)$_2$ / reduced graphene oxide composite as electrode for supercapacitors

V. Boychuk, V. Kotsyubynsky*, B. Rachiy, K. Bandura, A. Hrubiak, S. Fedorchenko

Vasyl Stefanyk Precarpathian National University, 57 Shevchenko str., Ivano-Frankivsk, 76018 Ukraine

Abstract

The electrochemical performance of Ni(OH)$_2$ / reduced graphene oxide nanocomposite obtained by ultrasonic treatment of hydrothermal synthesized β-Ni(OH)$_2$ and rGO has been investigated in alkaline medium. The material demonstrates good specific capacitance and is quite cost effective. The kinetics of proton migration in electrode materials has been investigated. The increasing of capacitance for Ni(OH)$_2$ / reduced graphene oxide composite up to 494 F / g in comparison with 121 and 133 F / g for rGO and Ni(OH)$_2$ at current density 0.08 A / g are attributed to the synergistic effect due to conductive system of graphene nanosheets formation and enhancement of both electron and ion transport.

Selection and peer-review under responsibility of the scientific committee of 3rd ISE Satellite Student Regional Symposium on Electrochemistry in Ukraine.

Keywords: nickel hydroxide, reduced graphene oxide, hybrid supercapacitor, proton migration, capacitance.

1. Introduction

Hybrid supercapacitors combine advantages of battery as an energy source (high energy density) and a capacitor as a power source (high current rate, good cycling) [1]. Fast Faradic reactions take place on one electrode and on the other one the electric double-layer (EDL) is formed as a result of electroactive particles absorption / desorption during charge / discharge processes. Hybrid (asymmetric) supercapacitors can use splitted potential windows of two

* Corresponding author. Tel.: +38-097-380-3959; fax: +38-034-253-1574.
E-mail address: kotsuybynsky@gmail.com

Selection and peer-review under responsibility of the scientific committee of 3rd ISE Satellite Student Regional Symposium on Electrochemistry in Ukraine.

electrodes that leads to widening of operation voltage and drastically increasing of both energy density and power density which are proportional to the working voltage squared. The working voltage is limited by electrolyte type. The organic electrolytes provide higher working voltage (up to 3 V), but specific capacitance of electrode materials in this case is lower due to the large sizes of the organic molecules which are associated with flammability, toxicity and high hygroscopicity. The aqueous electrolytes are comparatively cheaper and technologically simpler. They have high ionic conductivity of hydrated ions which are much smaller compared to ions solvated by organic electrolytes. The decreasing of potential window for aqueous electrolytes can be compensated by increasing of capacitance. Using of redox process for charge storage allows avoiding the main disadvantage of the carbon-based EDL supercapacitors – respectively low energy density. At the same time saving of good cyclic stability and long lifetime of battery-type electrode is an important problem. There is a wide range of perspective materials, such as RuO_2, MnO_2, MoO_3, V_2O_5, PbO_2, Co_3O_4, $Co(OH)_2$ and $Ni(OH)_2$ which have sufficiently high theoretical capacitances. One of the most promising is $Ni(OH)_2$ but low electrical conductivity and low cycle life restrict its using as pseudocapacitive material [2]. Using of metal hydroxide-carbon (nanofibers, graphene and reduced graphene oxides) composite electrodes can solve these problems [1].

2. Experimental details

Ultrafine β-$Ni(OH)_2$ is synthesized by hydrothermal treatment of sol obtained by the interaction of $NiCl_2 \cdot 6H_2O$ and ammonia solutions with the presence of polyethylene glycol (PEG) 6000 as a surfactant. The obtained precipitate is washed by distilled water until pH = 7 and dried at 60° C for 10 hours. Graphene oxide is synthesized by standard Hammers method. The reduction of graphene oxide (GO) is carried out under the hydrothermal conditions with the presence of hydrazine hydrate. β-$Ni(OH)_2$ / reduced graphene oxide (rGO) composite is obtained by ultrasound dispersing of β-$Ni(OH)_2$ and rGO (mass ratio of 2:1) in distilled water. Phase composition and crystalline structure of the synthesized materials are investigated by XRD (copper anode radiation, Bragg-Brentano scheme, DRON-3.0 diffractometer). The average size of coherent scattering domains (CSD) is calculated by Scherrer`s formula. Particle morphology is observed by SEM method (Vega 3 MLN TESCAN device). Porous structure and specific surface area are investigated by low-temperature nitrogen absorption (Quantachrome Autosorb Nova 2200e device). The electrical conductivity is investigated by impedance spectroscopy (Autolab PGSTAT 12/FRA- 2 device) for cylindrical samples prepared by pressing at 60 kN.

Electrochemical investigations are carried out in a three-electrode cell with a reference Ag/AgCl electrode, platinum wire as a counter electrode and a working electrode on the pure Ni grid. Working electrode consists of 90% active material, 5% acetylene black and 5% polyvinylidene fluoride mixed with n-methyl pyrrolidone and then dried to form a paste. Electrochemical performance is measured in 6 M KOH as an electrolyte. The specific capacitances are measured at specific currents in a range of 0.08-0.40 A / g. Cyclic voltammetry (CV) is carried out at scan rate of 0.5, 1, 2, 3, 4 and 5 mV s^{-1}. Electrochemical impedance spectra (EIS) are measured at frequencies from 0.01 Hz up to 100 kHz.

3. Results

Chemical reduction of graphene oxide using hydrazine leads to the removing of the functional (hydroxyl, epoxy, carbonyl) groups from the surfaces of graphene sheets with a possible restacking of rearrangement [3]. Under these conditions rGO sample is close to amorphous and only diffuse galo is fixed on XRD pattern in a range of 2θ=20-60° (Fig. 1). The local maxima are observed at 27 and 42° that corresponds to rGO structure [4].

The broadening of (001) reflex on the XRD pattern of β-$Ni(OH)_2$ is caused by the presence of nickel hydroxide particles with the sizes of about 30-40 lattice constants (15-20 nm) in the direction of *c* crystallographic axis. The presence of plane defects doesn't affect the width of this reflex [5]. This average crystallites` size is about 15 nm. On XRD pattern of $Ni(OH)_2$ / rGO composite the slight intensity increasing in the range of 25-30° is observed. Additionally (100) and (101) reflexes broadening that is caused by the presence of interplanar defects, is observed. It can be assumed that ultrasonic dispersion leads to the rGO fragments insertion into the interplanar space of β-$Ni(OH)_2$. The CSD average size of $Ni(OH)_2$ phase in composite material is about 13 nm.

Accordingly to SEM data initial rGO sample consists of graphene sheets packets (Fig. 2a) while initial β-$Ni(OH)_2$ sample is formed by spherical agglomerates with the sizes of about 1-2 μm (Fig. 2b). Carbon fragments are observed between the agglomerated $Ni(OH)_2$ particles for composite material (Fig. 2c). All the obtained materials have a well-developed mesoporous structure. Specific surface areas of rGO, β-$Ni(OH)_2$ and β-$Ni(OH)_2$/rGO are 402, 20 and 88 m^2 / g, respectively.

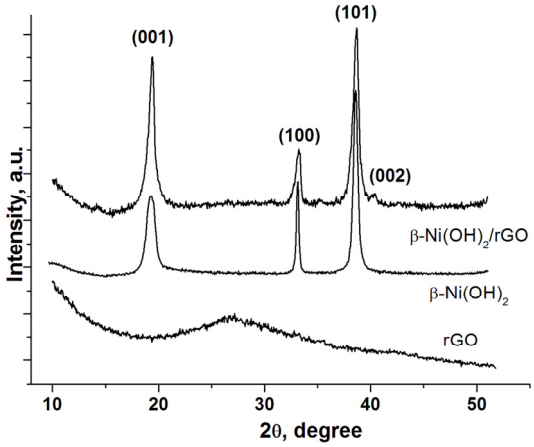

Fig. 1. XRD patterns of rGO, β-$Ni(OH)_2$ and β-$Ni(OH)_2$/rGO.

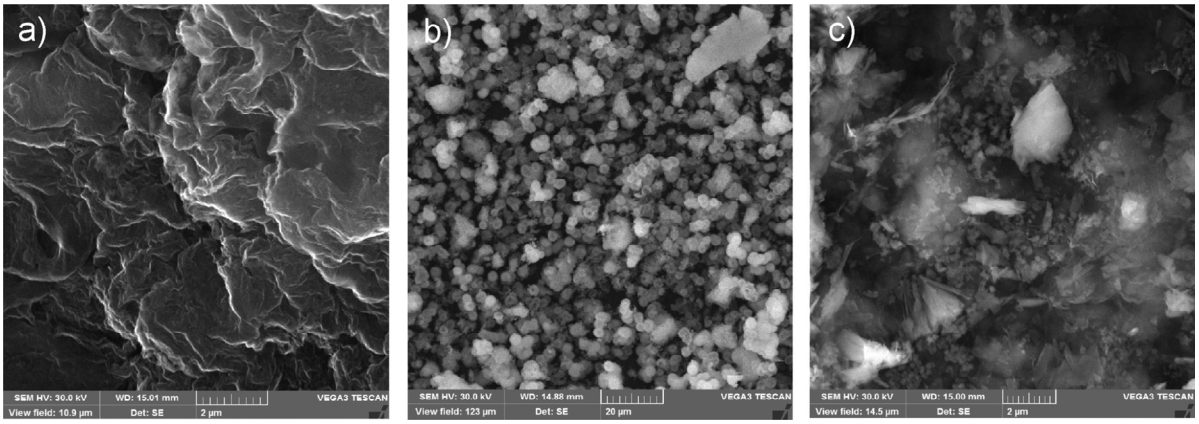

Fig. 2. The SEM images of (a) rGO, (b) β-$Ni(OH)_2$ and (c) β-$Ni(OH)_2$/rGO particles.

CV curves of rGO, β-$Ni(OH)_2$ and β-$Ni(OH)_2$/rGO are presented in Fig. 3. RGO electrode at all potential scan rates has close to rectangular cycles. This is the evidence of EDL mechanism of charge storage. The elliptical deformation of cycles can be explained by the presence of pseudocapacitive component due to the interaction of oxygen containing functional groups and H^+ ions. Only carbonyl and hydroxyl functional groups offer a pseudocapacitive effect in comparison with the other oxygen functional groups of graphene [6]. The specific capacitance *C* of the materials is calculated based on the CV measurements according to [7] using the equation:

$$C = \int_{U_1}^{U_2} I(U)dU / 2m\nu(U_2 - U_1) \quad (1)$$

where U_1 and U_2 are cutoff potentials in CV, $I(U)$ is a current, m is a mass of a sample, ν is a scan rate.

In contrast to rGO, which doesn't exhibit redox response, β-Ni(OH)$_2$ and β-Ni(OH)$_2$/rGO samples exhibit redox properties within a potential range from 0.0 to 0.5 V compared to Ag/AgCl as a result of Faradaic reactions on the surface of oxycation particles (Fig. 3 a).

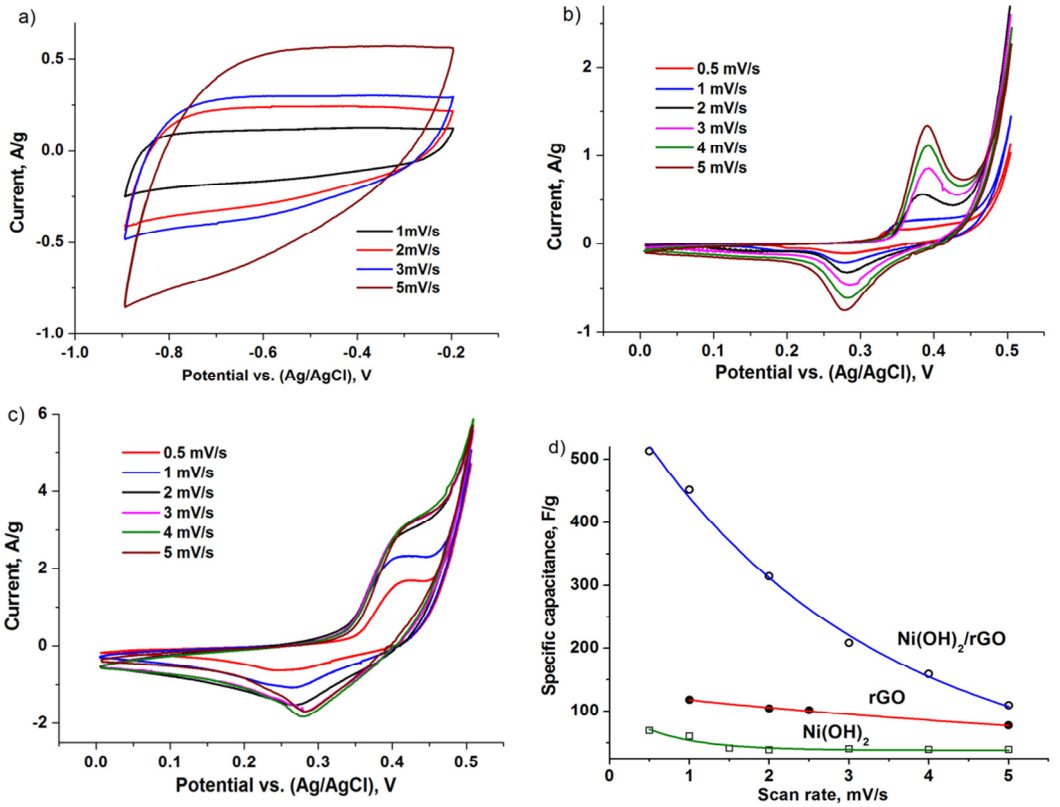

Fig. 3. Cyclic voltammograms at various scan rates for (a) rGO, (b) β-Ni(OH)$_2$ and (c) β-Ni(OH)$_2$/rGO electrodes (6 M KOH aqueous electrolyte) and (d) specific capacitance with scan rate.

The CV curve of composite electrode presents redox peaks in the same potential range observed for pure β-Ni(OH)$_2$ (Fig. 3 b,c). The redox peaks in alkaline electrolytes are caused by the transitions of hydrous nickel: $Ni(OH)_2 - e^- + OH^- \leftrightarrow NiOOH + H_2O$. The dominant mechanism of protonic conductivity for pure β-NiOH$_2$ is proton diffusion between localized protonic defects [8]. Hence high specific surface area and peculiarities of hydrothermal synthesis cause the presence of intercalated water molecules between stacked β-Ni(OH)$_2$ layers (Fig. 4). The interaction of water molecules and protons leads to the decreasing of proton detrapping energy as $Ni(OH)_2^+ - H^+ = NiOOH$ especially in the cases of the crystal disordering and possibility of electron transferring such as $Ni(OH)_2\text{-}e^- = Ni(OH)_2^+$. It is more probable for ultrafine β-Ni(OH)$_2$ particle in contact with rGO which is good electronic conductor. Specific conductivity of pure rGO used for composite preparation at 298 K is about 27 Sm / m while dc conductivities of β-Ni(OH)$_2$ and β-Ni(OH)$_2$/rGO samples are $9.0 \cdot 10^{-7}$ and $9.7 \cdot 10^{-5}$ Sm / m, respectively. Under these conditions the formation of hydroxonium ion (H_3O^+) at the interaction of free proton and intercrystalline water molecules. Unstability of H_3O^+ in alkali media leads to the detrapping of proton with the next its migration in the interlayer space via intermediate H_2O species and protonic defects. This mechanism, theoretically described in [9], predicts importance of additives with electronic conductivity which allows keeping effectiveness of proton transferring and minimize passivation effects influence of the charge / discharge process. The oxidation and reduction peaks for β-Ni(OH)$_2$ / rGO electrode are broadened and have higher specific current compared to the β-Ni(OH)$_2$. The potential of the anodic peak for β-Ni(OH)$_2$ / rGO shifts towards more positive potentials compared to the one for β-Ni(OH)$_2$ that is the evidence of the outer carbon layer contribution. This effect can be explained by the increasing of the internal resistance with the increasing of scan rate [10].

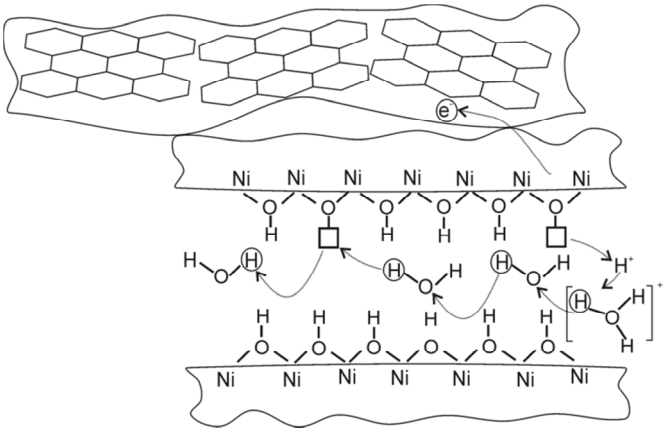

Fig. 4. Schematic representation of the proton migration in β-Ni(OH)$_2$

The contributions of EDL component and the redox component in charge storage capacity can be separated using different kinetic dependence of each capacity on potential scan rate (ν) [11]:

$$Q = Q_{\nu=\infty} + \alpha \nu^{-1/2} \text{ and } Q^{-1} = Q_{\nu=0}^{-1} + \alpha \nu^{1/2} \quad (2)$$

where Q is the total charge at different scan rates ($Q = Cm\Delta U = S/2\nu$, S is a total area of CV curves), $Q_{\nu=\infty}$ is a double layer charge and $Q_{\nu=0}$ is the maximum total charge that can be obtained and a and b are constants.

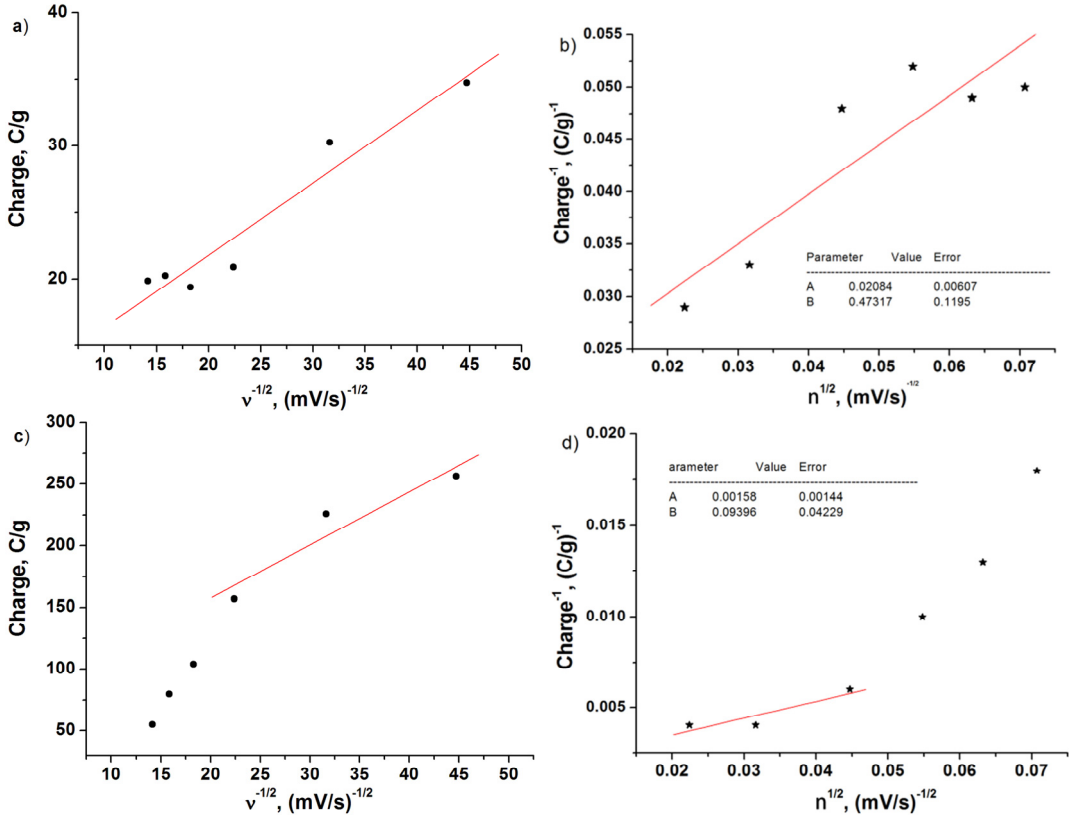

Fig. 5. The relation of charge (a, c) Q vs $\nu^{-1/2}$ and (b, d) Q^{-1} vs $\nu^{1/2}$ for (a, b) β-Ni(OH)$_2$ and (c, d) β-Ni(OH)$_2$/rGO.

Experimental dependencies Q vs $\nu^{-1/2}$ and Q^{-1} vs $\nu^{1/2}$ for β-$Ni(OH)_2$ (Fig. 5 a, b) and β-$Ni(OH)_2$/rGO (Fig. 5 c, d) were fitted with kinetic models at different scan rates that allows to calculate the contribution of redox capacitance. It was determined that pseudocapacitance type of charge accumulation is approximately 77-80% for β-$Ni(OH)_2$ electrode and 91 % for β-$Ni(OH)_2$ / rGO composite. The linear dependencies of the anodic and cathodic peaks current on the square root of scan rate (Fig. 6) is a result of the exhaustion of the electrode capacity for redox surface processes and indicates irreversible-like type of electrochemical system [12]. The deviation from an ideal electrochemical behavior is caused by respectively slow scan rate and slow charge / discharge process regulated by proton migration.

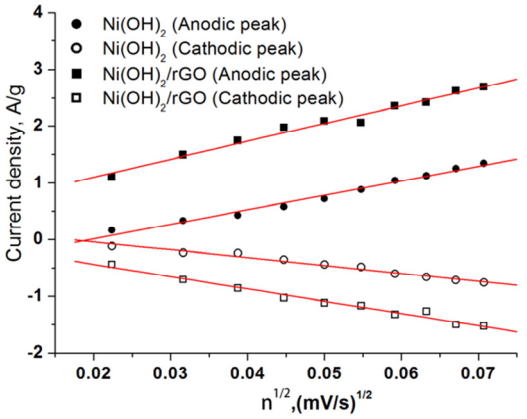

Fig. 6. The dependencies of peak current on the square root of scan rate for β-Ni(OH)2 and β-Ni(OH)2/rGO electrode.

Based on the scanning electronic microscopy (SEM) data we consider the next model: $Ni(OH)_2$ electrode consists of spherical particles with average sizes of about 1 μm that contact with the 3D-grid formed by randomly orientated fragments of rGO packets. It is assumed that average β-$Ni(OH)_2$ agglomerate size for composite electrode decreases to 250 nm due to ultrasonic treatment and electron transfer is realized through the carbon interparticles bridges. The polarization as a result of electrolyte concentration changes wasn't taken into account. It is considered that the migration length is close to average particle size and redox processes occur in all active particles of the electrode materials which contact with the liquid electrolyte when electron transfer occurs through β-$Ni(OH)_2$ / rGO interface. In this case the redox process are quasi-reversible electrochemical reactions and can be described by Randles–Shevchik equation [13]: $i = 2.69\times10^5 n^{3/2} A\Delta C D^{1/2} \nu^{1/2}$ (at 25° C), where i is a peak current, n is a number of electrons involved in electrochemical process ($n = 1$ for β-$Ni(OH)_2$), A is a surface area of the working electrode (cm^2), D is a diffusion coefficient of the protons (cm / s), C is a concentration of the protons (hydroxonium ions) in the electrolyte (mol / cm^3), ν is a scan rate (V / s). Surface area A and average number of particles in electrode can be evaluated using mass value of active material and an average density of β-$Ni(OH)_2$ (4.10 g / cm^3). The concentration of protons in the electrode is estimated using value of total charge transferred through the electrode during cycling.

Calculated proton electrostimulated diffusion coefficients D for the β-$Ni(OH)_2$ and β-$Ni(OH)_2$ / rGO electrodes in the case of anodic process are 1.5×10^{-11} and 2.6×10^{-11} cm^2/s, respectively, that correspond to [14]. In the case of cathodic process the diffusion coefficients D are smaller – 4.5×10^{-12} and 2.1×10^{-11} cm^2 / s. The diffusion coefficient for protons moving in the microcrystal hydrated nickel hydroxide lattice determined by a potential step cycling accordingly to [15] is somewhat higher – about $3.1\cdot10^{-10}$ cm^2 / s and $4.6\cdot10^{-11}$ cm^2 / s for charging and discharging processes, respectively. The decreasing of diffusion coefficient at the reduction stage for pure $Ni(OH)_2$ (about 7 times) is more larger then in the case of β-$Ni(OH)_2$ / rGO composite (about 1.3 times).

Better electrochemical performance of composite electrode in comparison with pure nickel hydroxide electrode and rGO (Fig. 3 d) indicates the existence of synergistic effects. Possible reasons of specific capacitance increasing for composite electrode are providing electrical contact of individual β-$Ni(OH)_2$ particles with interconnected fragments of graphene packages both with enlarging of Ni ions / electrolyte contact area and the improvement of proton mobility due to increasing of intercalated water amount.

The charge-discharge curves were measured in a potential window from 0 to 0.4 V under applied specific currents increasing from 0.08 A / g up to 0.40 A / g (Fig. 7). The plateau on the charge-discharge curves in potential range 0.25-0.32 V is a result of pseudocapacitive response and corresponds to reduction process identified by CV method. The discharge performance under the same conditions is better for β-$Ni(OH)_2$ / rGO compared to the pure β-$Ni(OH)_2$. The specific capacitance of the synthesized materials is calculated from the charge-discharge curves (obtained in three electrode configuration) using the following equation:

$$C_{spec} = \frac{I\Delta t}{m\Delta U} \tag{3}$$

where I is a constant discharge current and Δt is the discharge time, m is the mass of active materials (g), ΔU is the potential window of discharge.

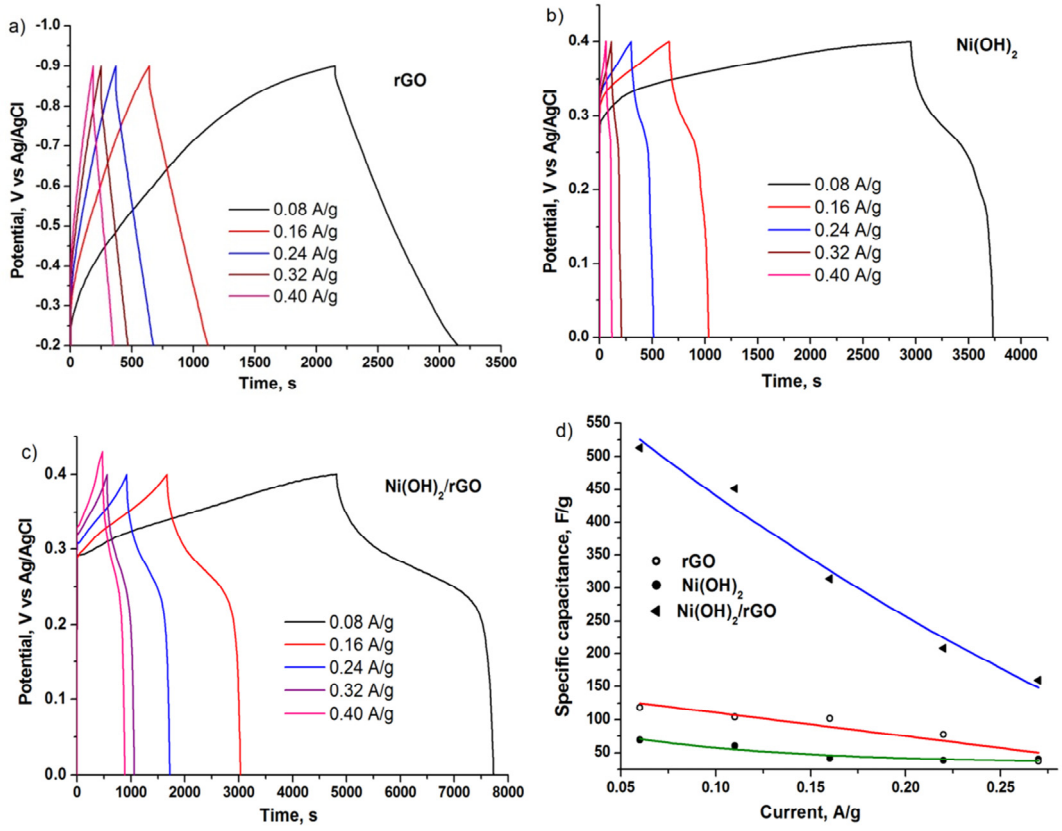

Fig. 7. Charge-discharge curves of (a) rGO, (b) β-$Ni(OH)_2$ and (c) β-$Ni(OH)_2$/rGO electrode at different current densities and (d) specific capacitance with used current density.

The β-$Ni(OH)_2$ / rGO electrode has higher specific capacitance compared to rGO and $Ni(OH)_2$ electrodes at all scan rates. The specific capacitance of composite is of about 494 F / g at the current density of 0.08 A / g in contrast to 121 and 133 F / g for rGO and $Ni(OH)_2$, respectively. The obtained values of C_{spec} (Fig. 6 d) are comparable with the data obtained at CV tests (Fig. 3 d). The specific capacitance for all the investigated materials decreases with the increasing of the current density but the decreasing rate is maximal for β-$Ni(OH)_2$ / rGO electrode. The capacitance of rGO and β-$Ni(OH)_2$ electrodes less depends on the applied current density.

The redox response of the active materials on the electrolyte / electrode interfacial surface is studied by EIS. Nyquist complex-plane plots are presented in Fig. 8. The impedance response measurements are performed at different biasing voltages which correspond to the used potential windows for obtaining of additional information about kinetic processes occurring in the electrodes. Nyquist plots for rGO electrode consist of broad semicircle in

the high and medium frequency region (result of charge transfer process at the electrode-electrolyte interface) and the straight line at the low frequency region (the diffusion transfer of electrically active particles). The starting point of semicircle determines of the internal resistance of a cells. The increasing of negative potential on the rGO electrode during EIS measurements leads to decreasing of high-frequencies semicircle.

Nyquist plots of β-$Ni(OH)_2$/rGO and β-$Ni(OH)_2$ electrodes consist of very small depressed semicircle and close to linear part in a range of low frequencies. The kinetics of the electrochemical systems is determined by the rate of the proton transferring. Linear dependence is violated for very low frequencies region. The angle of Warburg area is bigger for β-$Ni(OH)_2$ / rGO electrode that indicates that this electrode has comparatively lower charge transfer resistance and higher diffusion on the electrode-electrolyte interfaces.

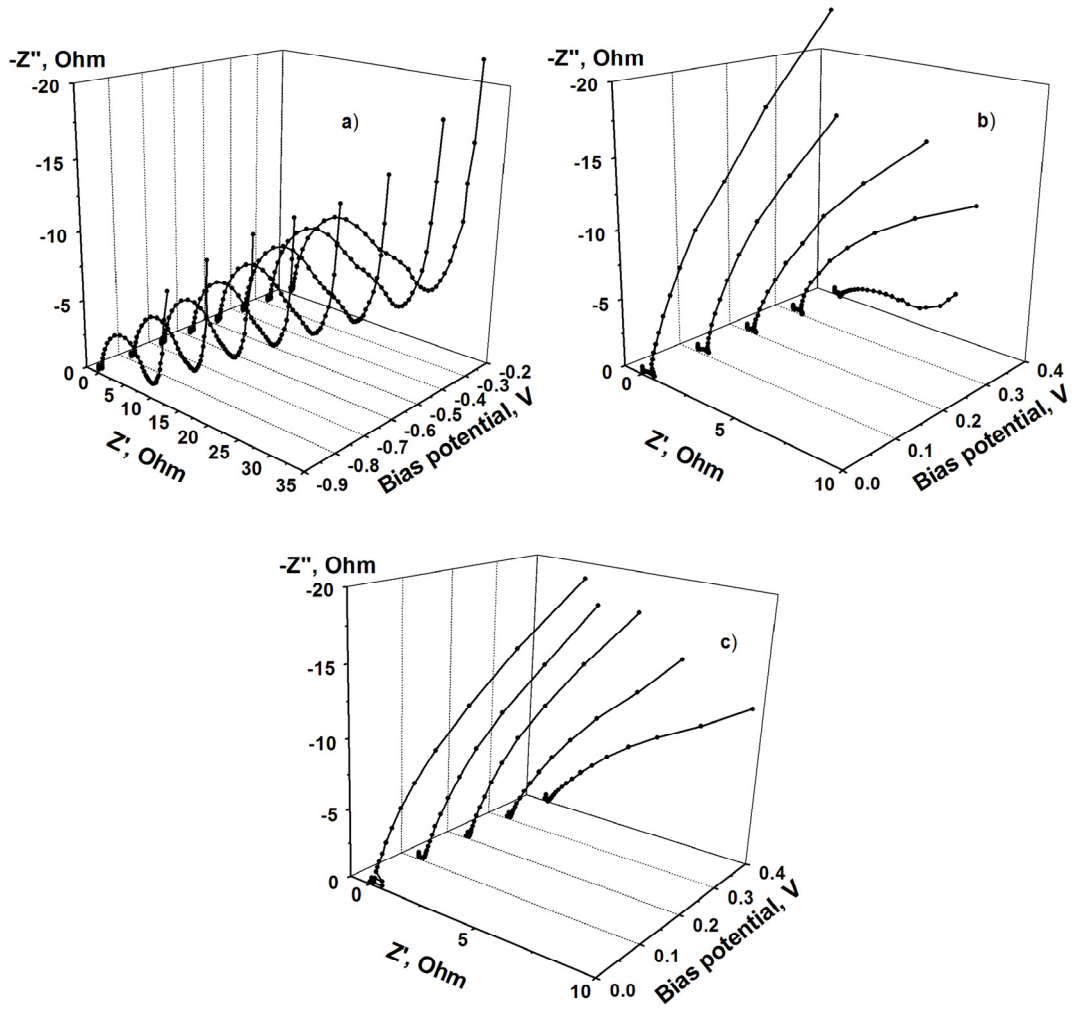

Fig. 8. Nyquist plots of (a) rGO, (b) β-$Ni(OH)_2$ and (c) β-$Ni(OH)_2$/rGO electrodes at the frequency range from 100 kHz to 0.01 Hz at different biasing potentials

The series resistance for β-$Ni(OH)_2$ / rGO electrodes are less than 0.1 Ω. The differences between Nyquist plots in a low frequencies area are caused by non-equilibrium character of electrically active particles transferring with the frequencies increasing. At low frequencies of Nyquist plot redox processes are controlled by the semi-infinite diffusion the magnitude of the impedance as follows [16]:

$$|Z| = \frac{l}{C_l (D\omega)^{1/2}} \tag{4}$$

where ω is a current frequency, l is an average diffusion path, C_l is a limiting capacitance and D is a diffusion coefficient for charge transport. Limiting capacitance C_l is determined as:

$$\frac{1}{C_l} = \frac{-dZ_i}{d(\omega^{-1})} \tag{5}$$

where Z_i is imaginary part of impedance. It is assumed that diffusion path l is close to average particle sizes. The exponential increasing of limiting capacitance at the bias potential increasing from 0 up to 0.4 V is observed for both β-Ni(OH)$_2$/rGO and β-Ni(OH)$_2$ electrodes (Fig. 9). The obtained values of proton electrostimulated diffusion (migration) coefficients at zero bias potential for Ni(OH)$_2$ and β-Ni(OH)$_2$/rGO are very close – 1.54×10^{-12} and 1.69×10^{-12} cm^2 / s, respectively. This result indicates the importance of double layer capacitance and diffusional capacitance for β-Ni(OH)$_2$ / rGO, which have better electrolyte accessibility and more sites for surface and bulk redox reactions as well as better possibility for proton mirgation.

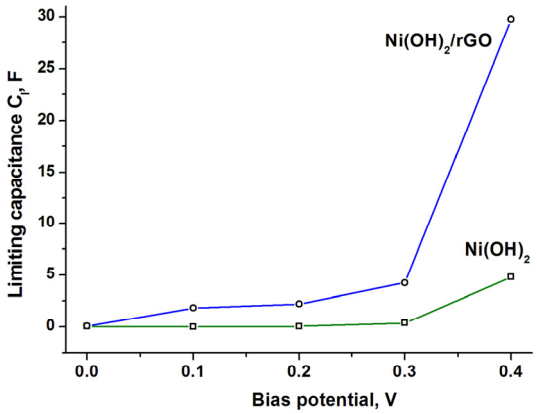

Fig. 9. Limiting capacitances versus bias potential for β-Ni(OH)$_2$ and β-Ni(OH)$_2$/rGO electrodes.

Energy and power densities are the key characteristics which determine the possibility of practical usage of supercapacitors. The relationship between energy densities and average power densities according to CV and charge / discharge measurements are calculated as follows: $E_{spec} = C_{spec}U^2 / 2$ and $W_{spec} = E_{spec} / t$, where C is an average capacitance calculated from the charge/discharge test, U is a working potential, and t is a discharge time.

A maximum energy density of about 17 W h / kg at a power density of about 20 W h / kg is achieved for β-Ni(OH)$_2$/rGO electrode (Fig. 10). According to Fig. 9 pseudocapacitance contribution is dominating for β-Ni(OH)$_2$ / rGO with the presence of good power density and due to high electric conductivity of 3D rGO grid which provide optimal paths for electron conduction. rGO electrode has power density up to 150 W / kg low depending on energy density. Pure β-Ni(OH)$_2$ has the lowest electrochemical performance.

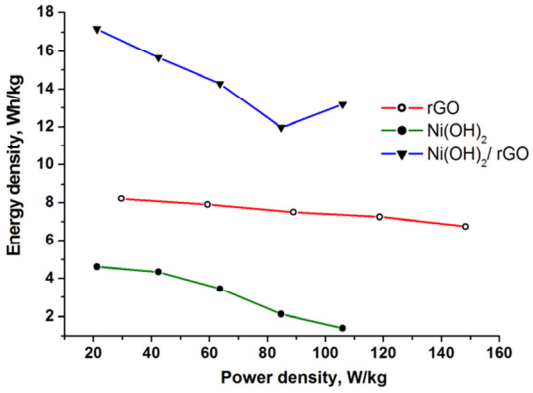

Fig. 10. Ragone plot of rGO, β-$Ni(OH)_2$ and β-$Ni(OH)_2$/rGO electrodes.

4. Conclusions

The electrochemical performance of β-$Ni(OH)_2$ / rGO nanocomposite obtained by ultrasonic treatment of hydrothermal synthesized β-$Ni(OH)_2$ and rGO has been successfully tested. The composite electrode demonstrates good specific capacitance – about 494 F / g at current density of 0.08 A / g compared to 121 and 133 F / g for rGO and $Ni(OH)_2$, respectively. The contribution of redox capacitance is approximately 77-80% for β-$Ni(OH)_2$ electrode and about 91% for β-$Ni(OH)_2$/rGO composite. The dominant mechanism of protonic conductivity for β-$Ni(OH)_2$/rGO composite where β-$Ni(OH)_2$ nanoparticles with intercalated water molecules are incorporated into electonic conducting 3D-grid formed by interconnected graphene packages is detrapping of proton with the next its migration in the interlayer space via intermediate H_2O species and protonic defects. The proton migration (electrostimulated diffusion) coefficient values (2.1-2.6)× 10^{-11} in 6 M KOH have been evaluated by cyclic voltammetry for $Ni(OH)_2$ / rGO. The capacitive increasing has been attributed to the synergistic effect of rGO and $Ni(OH)_2$: providing electrical contact of individual β-$Ni(OH)_2$ particles and graphene frame (important for proposed proton conductivity mechanism), enlarging of Ni ions / electrolyte contact area, the improvement of proton mobility due increasing of intercalated water amount. The energy density of $Ni(OH)_2$ / rGO electrode composite is about 17 W h / kg at the power density of about 20 W / kg.

References

[1] M. Zhi, C. Xiang, J. Li, M. Li, N. Wu, Nanoscale 5(1) (2013), 72-88
[2] S. R. Ovshinsky, M. A. Fetcenko, J. Ross Sci. 260(5105) (1993), 176-181.
[3] S. Pei, H. M. Cheng, Carbon 50(9) (2012), 3210-3228
[4] C. Fu, G. Zhao, H. Zhang S. Li, Int. J. Electrochem. Sci 8 (2013), 6269-6280.
[5] C. Tessier, P. H. Haumesser, P. Bernard, C. Delmas, J. Electrochem. Soc. 146(6) (1999), 2059-2067.
[6] B. Rajagopalan, J. S. Chung, Nanoscale Res. Lett. 9(1) (2014), 535.
[7] W. Chen, Z. Fan, L. Gu, X. Bao, C. Wang, Chem. Commun. 46(22) (2010), 3905-3907
[8] S. Motupally, C. C. Streinz, J. W. Weidner, J. Electrochem. Soc. 142(5) (1995), 1401-1408.
[9] S. Deabate, F. Henn, S. Devautour, J. C. Giuntini, J. Electrochem. Soc. 150(6) (2003) , J23-J31
[10] V.Z. Barsukov, B.E. Rogoza, L.N. Sagoyan, Sov. Electrochem. 20(12) (1984),1506 - 1510.
[11] J. Ji, L. L. Zhang, H. Ji, Y. Li, X. Zhao, X. Bai, R. S. Ruoff, ACS nano 7(7) (2013), 6237-6243.
[12] T. Nguyen, M. Boudard, M. J. Carmezim, M. F. Montemor, Sci. Rep. 7 (2017), 39980.
[13] H. Kanoh, Q. Feng, Y. Mi yai, K. Ooi, J. Electrochem. Soc. 142(3) (1995), 702-707.
[14] P. He, X. Zhang, Y. G. Wang, L. Cheng, Y. Y. J. Xia, Electrochem. Soc. 155(2) (2008), A144-A150.
[15] B. Shruthi, B. J. Madhu, V. B. Raju, S. Vynatheya, B. V. Devi, G. V. Jayashree, C. R. Ravikumar, J. Sci.: Adv. Mater. Devices 2(1) (2017), 93-98.
[16] C. Chur-Min, H. Hsuan-Jung, Anal. Chim. Acta 300(1-3) (1995), 15-23.